PCCP

ROYAL SOCIETY OF CHEMISTRY

PAPER

View Article Online
View Journal | View Issue

Cite this: *Phys. Chem. Chem. Phys.*, 2025, **27**, 12938

How the ionic liquid $[C_2C_1Im][OTf]$ affects the stability of Pt(111) during potential cycling†

Felix Hilpert, [a] Yunsheng Qiu,[b] Leopold Lahn,[cbd] Kevin Höllring,[e] Nicola Taccardi,[f] Peter Wasserscheid, [bf] Olga Kasian, [cbd] Ana-Sunčana Smith,[e] Karl J. J. Mayrhofer, [b] Valentin Briega-Martos, ‡[b] Serhiy Cherevko, [b] Olaf Brummel *[a] and Jörg Libuda [a]

Modifying electrocatalysts with ionic liquids (ILs) not only allows for precise control of selectivity but also often directly impacts the stability of the electrocatalyst. In this work, we study how the IL 1-ethyl-3-methylimidazolium trifluoromethanesulfonate $[C_2C_1Im][OTf]$ influences the electrochemical stability of the Pt(111) surface in acidic electrolyte (0.1 M $HClO_4$) during oxidation and reduction cycles (ORCs; 0.05–1.5 V_{RHE}). We used complementary electrochemical *in situ* methods, namely, cyclic voltammetry (CV), online inductively coupled plasma mass spectrometry (ICP-MS), and electrochemical scanning tunneling microscopy (EC-STM) in combination with an algorithmic pattern recognition approach. In the absence of the IL, Pt(111) dissolves during oxidative cycling *via* cathodic transient dissolution. In consecutive cycles, small Pt clusters are formed, which grow with increasing cycle number. In the presence of the IL, the dissolution rate increases by a factor of 5 and an additional anodic dissolution pathway occurs. The changes in the dissolution behavior during ORCs, however, have only minor impact on the morphological changes and the adsorption sites formed. We explain latter observation by the dominance of morphological changes due to the formation and reduction of an amorphous oxide layer, as opposed to dissolution and redeposition.

Received 28th January 2025,
Accepted 25th May 2025

DOI: 10.1039/d5cp00391a

rsc.li/pccp

Introduction

Ionic liquids (ILs) are successfully used as molecular modifiers both in heterogeneous catalysis[1,2] and electrocatalysis.[3–5] Numerous studies have demonstrated their ability to enhance catalytic activity, for example in the oxygen reduction reaction (ORR),[3,6–9] the oxygen[10,11] and hydrogen evolution reactions,[12] and the CO_2 reduction reaction (CO_2RR).[13,14] However, their greatest potential lies in the control of selectivity,[15–19] which can be tailored using the nearly limitless variety of available ILs.[20,21] These initial catalytic properties are directly entangled with the stability of the catalyst, which will be also affected by the modifier.[22]

A key mechanistic aspect of this selectivity control is the partial blocking of active sites—an inherent characteristic of IL-modified systems.[19,23–26] Notably, the most catalytically active sites, such as low-coordinated defect sites, are often also the least selective. By selectively blocking these defect sites, ILs can suppress undesired reaction pathways, and thereby, enhance the overall selectivity. These catalytic properties are closely linked to catalyst stability, which is likewise influenced by the presence of the IL modifier.[22]

For ORR electrocatalysts, stabilization has been reported for commercial Pt/C catalysts, preventing Pt dissolution, particle agglomeration, and carbon corrosion.[6,27–29] On the other hand, modification with ILs can also destabilize electrocatalysts. George *et al.*[9] showed this for PtNiMo/C electrodes and proposed that the IL suppresses the formation of a protective oxide layer. Endres and coworkers demonstrated that Au(111) undergoes restructuring in certain ionic liquids (ILs) due to the increased mobility of gold atoms, which depends on the applied potential.[30–32] This restructuring is strongly influenced by the specific properties of the ionic liquid.[30] In an recent

[a] *Interface Research and Catalysis, ECRC, Friedrich-Alexander-Universität Erlangen-Nürnberg, Egerlandstr. 3, 91058, Erlangen, Germany. E-mail: olaf.brummel@fau.de*
[b] *Forschungszentrum Jülich GmbH, Helmholtz Institute Erlangen-Nürnberg for Renewable Energy (IET-2), Cauerstr. 1, 91058, Erlangen, Germany*
[c] *Helmholtz-Zentrum Berlin GmbH, Hahn-Meitner-Platz 1, 14109, Berlin, Germany*
[d] *Department of Materials Science and Engineering, Friedrich-Alexander-Universität Erlangen-Nürnberg, 91058Martensstr. 5, Erlangen, Germany*
[e] *Institute of Theoretical Physics, Friedrich-Alexander-Universität Erlangen-Nürnberg, Cauerstr. 3, 91058, Erlangen, Germany*
[f] *Chair of Chemical Engineering, Friedrich-Alexander-Universität Erlangen Nürnberg, Egerlandstr. 3, 91058, Erlangen, Germany*

† Electronic supplementary information (ESI) available. See DOI: https://doi.org/10.1039/d5cp00391a

‡ Present address: Department of Chemistry and Chemical Biology, Cornell University, Ithaca, New York 14853, United States.

study, some of the authors could show that even small concentrations (10 mM) of the IL $[C_2C_1Im][DCA]$ enhances the Au dissolution during oxidation reduction cycling by more than 40 times, affecting directly the correlating morphology.[22] We assigned this to the specific adsorption both of the cation as well as the anion passivating the oxide formation and stabilization of dissolved Au ions due to complex formation with the IL.[22]

To understand catalyst stability at the molecular level, well-defined model systems are essential. One such system is the ionic liquid $[C_2C_1Im][OTf]$ in combination with Pt(*hkl*) single crystal surfaces, which has been extensively studied both under surface science conditions[33–36] and in electrochemical environments.[15–17,23] In our previous work, we demonstrated that $[OTf]^-$ anions adsorb onto Pt(111) in a potential-dependent and largely reversible manner. This specific adsorption behavior can be harnessed to modulate electrocatalytic selectivity.[23] For instance, during the oxidation of 2,3-butanediol—a secondary alcohol with two hydroxyl groups—the IL shifts the selectivity toward the intermediate acetoin, in which only one alcohol group is oxidized,[15,16] while also suppressing CO formation typically observed on Pt(100).[16] Moreover, even low concentrations of the IL have been shown to selectively suppress one of two competing reactions.[17]

This robust body of work establishes $[C_2C_1Im][OTf]$ on Pt(111) as a highly suitable model system for probing ionic liquid–surface interactions under electrochemical conditions. Given the vast structural diversity of ionic liquids, systematic studies of such representative systems are critical for developing generally applicable design principles.

While the mechanisms of activity and selectivity control in this system are well understood, the effect of $[C_2C_1Im][OTf]$ on the electrochemical stability of Pt electrodes has remained unexplored. Here, we address this knowledge gap by investigating how this IL influences the stability of Pt(111) in aqueous electrolyte during consecutive oxidation and reduction cycles (ORCs). As schematically illustrated in Fig. 1, we employ a complementary suite of *in situ* electrochemical techniques—including cyclic voltammetry (CV), online inductively coupled plasma mass spectrometry (ICP-MS), and electrochemical scanning tunnelling microscopy (EC-STM)—together with algorithmic pattern recognition.

Although the presence of the IL leads to enhanced Pt dissolution during ORCs, it does not result in significant changes in surface morphology or the formation of new adsorption sites. Our findings suggest that surface roughening primarily arises from rearrangements associated with the formation and reduction of the amorphous oxide layer, rather than from dissolution and redeposition of Pt.

Notably, this is the first example of a system in which a surface modifier that significantly influences electrocatalytic selectivity[15–17] has only a minimal impact on electrode stability under identical conditions. This unique combination of high selectivity control with low degradation renders the system a particularly valuable reference point and offers new design criteria for the development of stable, IL-modified electrocatalytic interfaces.

Experimental methods

Cleaning procedure

We stored all glass and polytetrafluorethylene (PTFE) parts used in the CV and EC-STM experiments, in a solution of concentrated sulfuric acid (Merck, Emsure, 98%) and NOCHROMIX® (Sigma-Aldrich) overnight. Before each measurement, we performed three consecutive rinsing (5 times) and boiling (for 30 minutes) cycles with ultrapure water (Milli-Q Synergy UV, 18.2 MΩ cm at 25 °C, TOC < 5 ppb).

Preparation of Pt electrodes and solutions

Pt(111) single crystals. We annealed Pt(111) single crystals (MaTecK, 99.999%, depth of roughness < 0.01 μm, accuracy of orientation < 0.4°) in the blue flame of a Bunsen burner for 2 minutes. The crystals were cooled down in Ar/H_2 (Ar: Linde

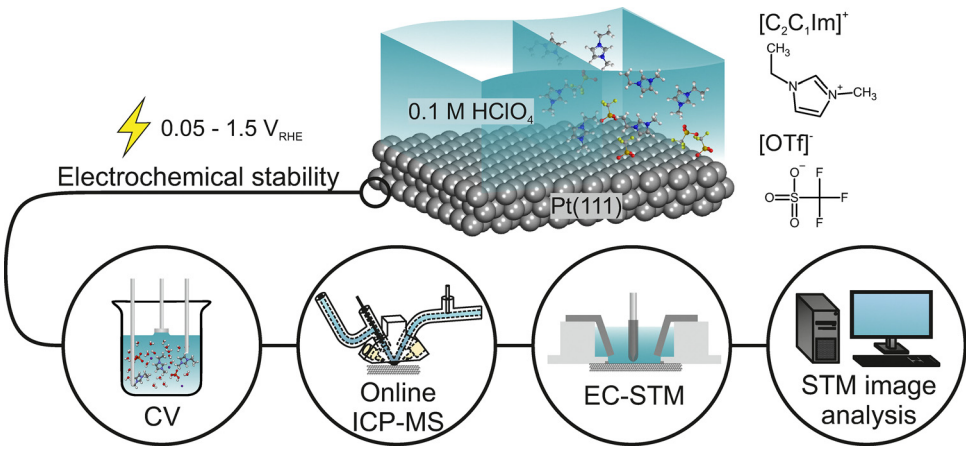

Fig. 1 Electrochemical system studied in this work. Stability of Pt(111) in 0.1 M $HClO_4$ in absence and presence of the ionic liquid $[C_2C_1Im][OTf]$. We probe the electrochemical stability of the system applying CV, online ICP-MS, EC-STM and using an algorithmic pattern recognition approach to analyze STM images.

5.0, H_2: Linde 5.3; volume ratio of $\sim 3:1$) atmosphere to room temperature.

Polycrystalline Pt. An approximately 200 nm thick polycrystalline Pt thin film sample was deposited onto a Si-Wafer substrate (Siegert Wafer GmbH, Germany) using a high-vacuum magnetron sputter system (Bestec, Germany). The base pressure in the main chamber before deposition was below 5.0×10^{-6} Pa. Ar (99.9999%) was used as the sputter gas and the pressure in the chamber was adjusted to 0.50 Pa at room temperature. A uniform adhesion layer of 15 nm metallic Ti was applied before deposition of Pt, which was carried out at a power of 100 W and constant rotation speed of 30 rpm using a 3-inch diameter Pt target (99.95%, Evochem, Germany). The resulting thin film was plasma cleaned in the high-vacuum of the main chamber and subsequently used as the working electrode in the online ICP-MS setup.

Solutions. We prepared solutions of $HClO_4$ (Roth, Rotipuran Ultra 70% or Merck Suprapur®) and $[C_2C_1Im][OTf]$ using ultrapure water (Milli-Q Synergy UV, ELGA PURELAB, 18.2 MΩ cm at 25 °C, TOC < 5 ppb). The IL was synthesized and purified in-house as previously described.[23] We degassed all solutions by purging with N_2 (Linde, 5.0) or Ar (5.0) for at least 20 minutes.

Cyclic voltammetry

We recorded CVs with a Gamry Reference 600+ potentiostat in hanging meniscus configuration in a three-electrode setup. We used a Pt wire (Mateck 99.9%) as CE and a freshly prepared RHE as reference electrode. We prepared the RHE in 0.1 M $HClO_4$ prior to each experiment. A potential of 12.5 V was applied between the CE and the platinum wire of the RHE until it was filled halfway with hydrogen. For the IL containing solution, the RHE was prepared in 0.1 M $HClO_4$ electrolyte, and the IL was added afterwards. We alternated ORCs (0.05–1.5 V_{RHE}, scan rate 50 mV s^{-1}, total number of 1, 3, 10, 20 and 40 cycles) and characterization cycles (0.05–0.9 V_{RHE}, scan rate 50 mV s^{-1}) in two separated cells. The characterization cell contained 0.1 M $HClO_4$, while the ORC cell contained 0.1 M $HClO_4$ in absence or presence of 1 M $[C_2C_1Im][OTf]$. After ORC, the crystal surface was cleaned in a beaker with ultrapure water. The crystal surface was protected by a droplet of ultrapure water during each transfer. Before each characterization, we performed an additional cleaning step developed in this work (see ESI,† Section 2 for details) inside the characterization cell, where we cycled the potential 16 times between 0.05 and −1.0 V_{RHE} at 50 mV s^{-1}. Afterwards, we purged the solution of the characterization cell for 5 minutes with N_2.

Electrochemical online ICP-MS

The real-time mass spectrometry analysis of Pt dissolution was conducted using customized scanning flow cells (SFCs)[37] hyphenated to an ICP mass spectrometer (PerkinElmer Nexion 350X). Details about the SFC-ICP-MS technique's design and operating principles are provided in previous publication.[38,39] Pt(111) and polycrystalline Pt thin films (200 nm) deposited onto Si-wafers were used as working electrodes in contact with the SFC configuration designed respectively for Pt(111) single crystal electrode (contacting area: *ca.* 0.16 cm^2), and for polycrystalline Pt film (contacting area: *ca.* 0.01 cm^2). The approaching of the working electrode to the SFC-ICP-MS setup was realized with a YXZ-translation stage (3 × M-403.6 DG, Physik Instrumente) Glassy carbon (for single crystal) or graphite (for polycrystalline Pt) rods were used as counter electrodes and Ag/AgCl (3 M KCl, Metrohm) as reference electrode. The flow rate through the SFC cell was *ca.* 3.5 μL s^{-1}. To study the ionic liquid effect on the stability of Pt(111), 10 mM $[C_2C_1Im][OTf]$ was added to 0.1 M Ar-saturated $HClO_4$ electrolyte. The electrochemical measurements were conducted using a Gamry (Reference 600) potentiostat. All SFC components, gas flow and the potentiostats were controlled by in-house developed LabVIEW (National Instruments) programs. For the mass calibration of Pt, a calibration curve of four points (0, 0.5, 1, 5 μg L^{-1}) was obtained using different Pt-concentrated standard solutions (Merck, Certipur). 10 μg L^{-1} Re (Merck, Certipur) was constantly monitored as internal standard. The RHE potential was measured on a Pt reference sample against the Ag/AgCl 3 M KCl reference electrode in H_2 saturated 0.1 M $HClO_4$ before the measurements. The RHE scale is used to present all potentials published in this work. The applied protocol consisted of two CVs from 0.05 (for Pt(111)) and 0.1 (for Pt_{poly}) to 1.5 V_{RHE} with a scan rate of 10 mV s^{-1}. The delay between the electrochemical signal and the corresponding mass spectrometry response was approximately 20 s. This delay was determined through separate pulse experiments using sufficiently positive potentials to induce immediate electrochemical dissolution. After applying this correction, a direct correlation between the electrochemical and mass spectrometry signals is achieved.[40]

EC-STM

We measured EC-STM images using a Keysight Technologies (Series 5500 AFM/SPM) STM equipped with a bipotentiostat. The EC-STM is isolated from vibrations by a combination of active and passive noise damping systems. We placed the Pt(111) crystal on the bottom of a home-built electrochemical PTFE-cell with a volume of 0.8 mL and sealed the cell with an O-ring (Kalrez®). During the measurements, we mounted the EC-STM cell in an environmental chamber purged with N_2 (5.0, Linde). A flame annealed Pt wire (MaTecK, 99.9%) served as a counter electrode and a Pd/H electrode (Pd wire 1 mm, MaTecK, ≥99.98%) as reference electrode. We prepared the Pd/H reference electrode following the procedure reported in the literature,[41] with full details provided in Section 4 of the ESI.† We refer all potentials of the EC-STM experiment against the RHE. We used 0.1 M $HClO_4$ in absence and presence of 1 M $[C_2C_1Im][OTf]$ as supporting electrolyte.

We etched electrochemically platinum iridium (80/20, 0.25 mm diameter) tips following a procedure adapted from Friebel *et al.*[42] (2 M KOH and 4 M KSCN, 1 kHz rectangular voltage of 10 V_{PP} + 2 V_{DC}). The tips were subsequently coated with Apiezon wax (Apiezon WAX W, Apiezon) to minimize faradaic currents on the tip. We measured in constant current mode with tunnelling currents ranging from 0.2 to 1 nA. The tip potential was kept constant during scanning at −0.35 V_{RHE} and the sample potential at 0.1 V_{RHE}. For cycling, we set scan rates

of 50 or 400 mV s^{-1} for the experiments with 40 and 800 cycles, respectively. We retracted the tip out of the solution during potential cycling to negate a local drain for soluble Pt species. We provide further details on the EC-STM setup in our previous publication.[43] We post processed the EC-STM images (data levelling, row aligning) with the Gwyddion software (version 2.64).[44]

Image evaluation, object size detection and statistical analysis

The original STM images were converted to grayscale. To improve contrast and visibility of individual objects, scarring artifacts were removed using Gwyddion software[44] and (bi)linear bias were removed from the background. The greyscale images were exported as TIF files for further processing to avoid compression losses. Using a custom python script that was originally developed to detect cell nuclei in greyscale images, we identified the objects on top of the pre-processed surface image, their positions and characteristic sizes. We compared these results with those obtained from the application of the object instance detection by watershed segmentation provided by the Gwyddion software and found excellent agreement. Therefore, for statistical analysis and to facilitate reproducibility by other groups, we used the resulting particle sizes obtained by Gwyddion with default settings as the basis.

Results and discussion

Cyclic voltammetry

In a first step, we used cyclic voltammetry to characterize the stability of the Pt(111) surface after ORCs in the absence and presence of the IL $[C_2C_1Im][OTf]$. The measurement protocol is shown schematically in the middle panel of Fig. 2 and consists of a characterization step, an ORC step and a cleaning step.

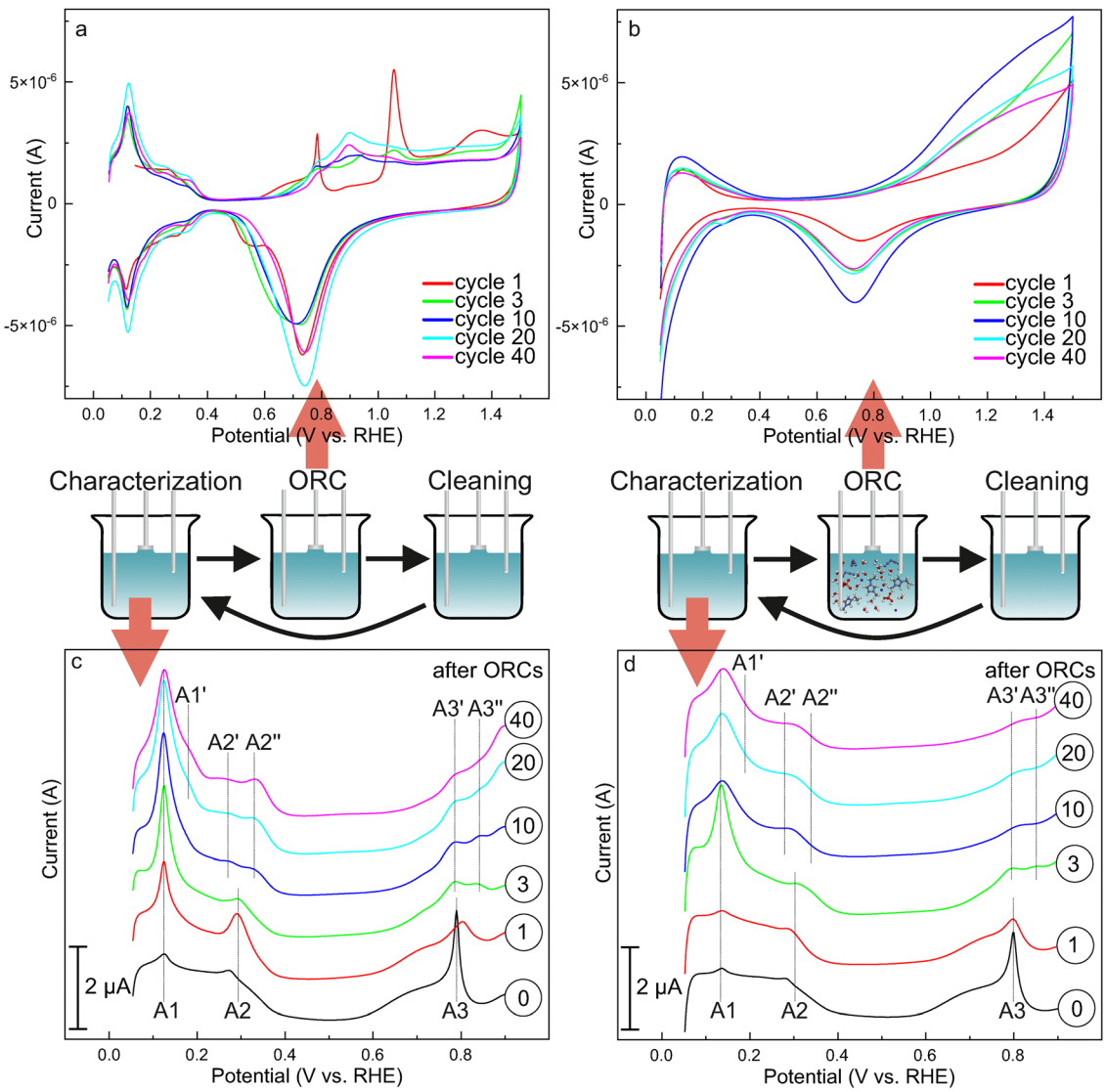

Fig. 2 Cyclic voltammograms of Pt(111) during ORCs (0.05–1.5 V_{RHE}, 50 mV s^{-1}) in the absence (a) and presence (b) of 1 M $[C_2C_1Im][OTf]$. Corresponding characterization CVs (0.05–0.9 V_{RHE}, 50 mV s^{-1}) measured after ORCs in absence (c) and presence (d) of IL in blank electrolyte only (0.1 M $HClO_4$). An additional cleaning step was performed between the ORCs and the characterization.

First, the crystal was characterized in a non-oxidative regime (between 0.05 and 0.9 V_{RHE}) in blank electrolyte (0.1 M $HClO_4$). Note that such CVs are highly sensitive to changes in the surface structure as well as to the presence of adsorbates.[45–48] Next, we transfer the crystal to a second electrochemical cell and perform ORC from 0.05 to 1.5 V_{RHE}. We did this in the absence or presence of the IL. Before the following characterization step, we cleaned the sample by reductive cycling (0.05 to −1.0 V_{RHE}, 50 mV s^{-1}, 16 cycles) to remove adsorbed IL or possible decomposition products and to establish comparable conditions for the characterization between the ORCs in the absence and presence of the IL [C_2C_1Im][OTf] (see ESI,† Section 2 for details). We measured characterization CVs in blank electrolyte before the ORCs and after cycles 1, 3, 10, 20 and 40.

A comparison of the results for experiments in absence and presence of the IL is shown in Fig. 2. Before discussing the characterization CV of Pt(111) treated by ORCs in the absence and presence of the IL, we will first discuss the CVs recorded during the ORCs. In the absence of IL, we observe in the anodic scan of the first cycle (red) three regions between 0.05 and 0.9 V_{RHE}, the so-called hydrogen, double layer and butterfly regions. We will describe and discuss these features and their development in detail when discussing the characterization CVs. Above 0.9 V_{RHE} we observe a sharp feature at 1.05 V_{RHE} and a broader feature at 1.35 V_{RHE}. These features are attributed to the formation of O_{ads} on Pt(111) and the formation of an amorphous bulk oxide layer, respectively.[47,49] In the cathodic scan, we observe two reduction peaks above the hydrogen region, at 0.74 and 0.56 V_{RHE}, which are attributed to the reduction of platinum oxide (PtO) and the desorption of subsurface oxygen (O_{ss}), respectively.[47,49] All features are in perfect agreement with previous work on Pt(111).[50] With increasing cycle number, the anodic scan features at 1.05 and 1.35 V_{RHE} decrease and several new peaks appear between 0.7 and 1.2 V_{RHE}. In the cathodic scan, the second reduction peak at 0.56 V_{RHE} disappears with increasing cycle number and the reduction peak at 0.74 V_{RHE} first broadens and shifts to lower potential. At cycle 10 and above, the peak becomes sharper again and shifts back to higher potentials. All these observations indicate that a variety of different adsorption sites are formed during potential cycling.

To get a more detailed picture of the adsorption sites, we analyzed in detail the characterization CVs measured within the stability window of Pt(111) (0.05–0.9 V_{RHE}). In the CV measured before the first ORC, we observe a flat hydrogen region between 0.05 and 0.4 V_{RHE} with only very small peaks at 0.12 (A1) and 0.29 V_{RHE} (A2). The double layer region between 0.4 and 0.6 V_{RHE} is featureless. The butterfly region between 0.6 and 0.9 V_{RHE} shows the well-known shape of Pt(111)[51] with a sharp peak at 0.8 V_{RHE} (A3). The hydrogen region of Pt(111) is assigned to the consumption/formation of H_{ads} in the anodic/cathodic scan. The features at 0.12 and 0.29 V_{RHE} were originally assigned to hydrogen adsorption/desorption on {110} and {100} step sites, respectively.[51] However, studies by Koper *et al.* suggest that the origin of these features also involves an exchange of H_{ads} by OH_{ads} species at these step sites.[52–56] The capacitive behavior of Pt(111) in the region of the double layer is still the subject of investigation.[57] The butterfly region is assigned to the adsorption of OH_{ads} induced by the activation of water. The origin of the sharp feature at 0.8 V_{RHE} is proposed to be the adsorption of two different types of water[46,58] or a disorder order phase transition.[48] All features are indicative of a well-ordered defect lean surface in clean electrolyte.

After the first ORC, the features at 0.12 (A1) and 0.29 V_{RHE} (A2) increase significantly. The sharp feature at 0.8 V_{RHE} (A3) in the butterfly region starts to become broader and less intense. After 3 cycles, the peak at 0.12 V_{RHE} (A1) continues to increase in intensity, while the peak at 0.29 V_{RHE} (A2) decreases in intensity. The weak peak in the butterfly region splits into two features at 0.78 (A3′) and 0.84 V_{RHE} (A3″). After 10 cycles the peak at 0.12 V_{RHE} (A1) becomes broader, and an additional shoulder appears at 0.17 V_{RHE} (A1′). Also, peak A2 splits into two features at 0.27 (A2′) and 0.33 V_{RHE} (A2″). As the number of cycles increases, the features at 0.17 (A1′) and at 0.33 V_{RHE} (A2″) become more intense.

From the observation that both features at 0.12 and 0.29 V_{RHE} become more intense after the first ORC, we conclude that {110} and {100} defects form initially. In the subsequent cycles, the peak at 0.12 V_{RHE} corresponding to {110} defects is dominant and also the additional feature in the butterfly region at 0.8 V_{RHE} is attributed to {110} defect sites,[47] indicating that these steps are formed preferentially. Note that this observation is consistent with previous work,[47,59,60] which ascribe the preferential formation of {110} defects to differences in formation energies between {110} and {100} sites due to surface strain relaxation.[47] Finally, we attribute the splitting of the peaks A1 (at 0.12 V_{RHE}) and A2 (0.29 V_{RHE}) into A1 (0.12 V_{RHE}) and A1′ (0.17 V_{RHE}) and A2′ (0.27 V_{RHE}) and A2″ (0.33 V_{RHE}) at cycle numbers $\geq$ 10 to the additional formation of {110} and {100} facet sites, as it is known for Pt nanoparticles. We will return to this point when discussing the *in situ* STM images of the system.

When performing the ORC of the Pt(111) surface in the presence of 1 M [C_2C_1Im][OTf], we observe distinct differences compared to the situation in the absence of the IL. In the anodic scan of the initial cycle the hydrogen region is partially blocked and the features from the butterfly are fully suppressed. The sharp feature observable in the absence of the IL at 1.05 V_{RHE} assigned to the formation of O_{ads} is not detectable anymore. The feature assigned to the formation of an amorphous bulk oxide at 1.35 V_{RHE} is also partially blocked and shifted to higher potentials. In the cathodic scan only one reduction peak is observable. Also in the cathodic scan, the hydrogen region is partially blocked, and the feature assigned to the presence of {110} and {100} defects is completely missing. The features assigned to the defect sites in the hydrogen region are also missing in the consecutive cycles. With increasing cycle number, we observe first a distinct increase in the total charge of the region assigned to O_{ads} and bulk oxide formation between 0.9 and 1.5 V_{RHE} and the peak assigned to the reduction of the oxide at 0.74 V_{RHE}. This charge reaches a maximum after 10 cycles and decreases slightly afterwards and stabilizes.

The same trend is also observable for the hydrogen region, however, to a much weaker extent. In previous work we could show that the $[OTf]^-$ anion of the IL adsorbs specifically on the Pt(111) surface in a potential-dependent and mainly reversible manner.[23] We assign the decrease of the charges in the hydrogen and oxygen region to the specific adsorption of the [OTf] ion. Note that we do not exclude additional contributions also from decomposition products of the IL catalyzed by the Pt(111),[34] as well as trace contaminations present in the IL. As the features attributed to the {110} and {100} defect sites are completely suppressed, we conclude that the anion adsorbs preferentially to the low coordinated Pt defect sites and blocks particularly these sites. Note that these low coordinated sites are typically also the most unselective sites and blocking of these sites by IL is used to increase selectivity.[2,61]

To analyze the effect of the presence of the IL during ORC on the surface structure of the Pt(111) electrode, we measured characterization CVs in blank electrolyte in the stability window of Pt (between 0.05 and 0.9 V_{RHE}). To obtain results, which are directly comparable to the sample treated in the absence of the IL, we implemented an additional cleaning step, in which we cycled 16 times between 0.05 and −1.0 V_{RHE} with a scan rate of 50 mV s^{-1} (see ESI,† Section 2 for details) to remove remaining adsorbates present in the IL experiment. Note that the same cycling step was also applied in the experiment in the absence of the IL.

The characterization voltammogram of the freshly prepared Pt(111) surface before contact with the IL solution or any ORC exhibits again the characteristics of a well-ordered Pt(111) surface. Specifically, this is the flat hydrogen region with only minor contributions from {110} (A1, 0.12 V_{RHE}) and {100} step sites (A2, 0.29 V_{RHE}) and the characteristic butterfly in the oxygen region with a sharp peak at 0.8 V_{RHE}, as discussed for the reference experiment. After the first ORC in presence of the IL, the peaks A1 and A2 show less growth, compared to the situation in the absence of the IL, whereas the butterfly peak A3 shows a similar broadening and decrease in intensity as in the experiment without the IL. After 3 ORCs, the CV is consistent with the situation without the IL. Peak A1 at 0.12 V_{RHE} grows significantly, A2 is present, and A3 splits into two features at 0.79 (A3′) and 0.84 V_{RHE} (A3″). After 10 cycles and above, peak A1 becomes broader and the shoulder A1′ is less evident compared to the experiment without IL. Also, the two features A2′ and A2″ are less apparent and can be identified as one broad peak A2. The two features A3′ and A3″ are less clearly identifiable as the intensity is decreased and peak shapes are broadened to a point where they appear to be one peak. But in general, the characterization CVs measured after ORCs in the absence and the presence of the IL are quite similar.

The consistency of the features of Pt(111) measured in the voltammograms before ORCs for both samples confirm the initial presence of well-ordered Pt(111) surfaces. We attribute the discrepancy of A1 and A2 intensity after the first cycle to slightly different initial nucleation (see discussion about STM images) or the blocking of specific defect sites by residual adsorbates (remaining IL, decomposition products of the IL catalyzed by the Pt(111) surface,[34] and/or contaminations). Since the outcome for peak A3 is the same for the experiment with and without IL, we assume a similar decrease in surface order. This assessment is further supported by the observation that after 3 ORCs, the fingerprint structure of the characterization CVs for both experiments is very similar. We also observe the preferential formation of {110} defect sites. The peaks after 10 cycles and more have the same positions and show similar evolution as in the experiment in the absence of IL, but are more damped, most likely caused by residual adsorbates or minor differences in the particle growth. We summarize the CV experiments that we observe specific adsorption of the [OTf] anions with the Pt(111) surface and especially low coordinated Pt sites. However, this interaction has little effect on the evolution of the Pt(111) surface during ORCs in terms of defect and facet formation compared to the situation in the absence of IL.

Electrochemical online ICP-MS

In order to identify the effect of the IL $[C_2C_1Im][OTf]$ on the dissolution behavior, we investigated in the next step the Pt(111) surface during ORCs using online ICP-MS, both in the absence and presence of 10 mM $[C_2C_1Im][OTf]$. We recorded two consecutive cycles between 0.05 and 1.5 V_{RHE}, with 10 mV s^{-1} and followed the Pt dissolution. As a reference experiment, we performed the same procedure also on polycrystalline Pt. The results are presented in Fig. 3. Extracting from the logarithmic plot of the Pt(111) dissolution (Fig. S1, ESI†), in the absence of the IL, the dominating dissolution profile appears in the cathodic process on Pt(111) surface, the anodic dissolution onset is *ca.* 1.22 V_{RHE}. Note that this is specific for the single crystalline Pt(111) surface,[39] while the polycrystalline Pt surface shows besides the cathodic dissolution peak (9.0 ng cm^{-2}) also a pronounced anodic dissolution peak (1.1 ng cm^{-2}) with an onset at *ca.* 1.0 V_{RHE}. On Pt(111) the dissolution increases from the first to the second cycle, from 0.40 to 0.75 ng cm^{-2}, which is again in direct contrast to the polycrystalline surface, where the Pt dissolution is practically identical in the two consecutive cycles (see Fig. S2, ESI†). On Pt(111) and in the presence of the IL, we observe an increase in Pt dissolution from the first to the second cycle, which is specific for the single crystalline surface. The enhancement of Pt dissolution is more noticeable in the presence of the IL. On Pt(111) the dissolution is enhanced by a factor of *ca.* 5 (1.76 and 3.83 ng cm^{-2} in the first and second cycle), and also a significantly enhanced anodic Pt dissolution is observed in the presence of IL (see semi-logarithmic representation in Fig. S1 for details, ESI†), with a dissolution onset shifted negatively to *ca.* 1.15 V_{RHE}. On polycrystalline Pt, the increase in dissolution in the presence of the IL is less pronounced but with a factor of 1.5, still strong.

In general, the anodic dissolution peak is attributed to the transient dissolution that occurs during the formation of the surface oxide, while the more pronounced cathodic dissolution peak is attributed to the transient dissolution during the reduction of the Pt surface oxides.[62,63] We assign the increased Pt dissolution in consecutive cycles to the formation of low coordinated Pt sites at the {110} and {100} steps during the first

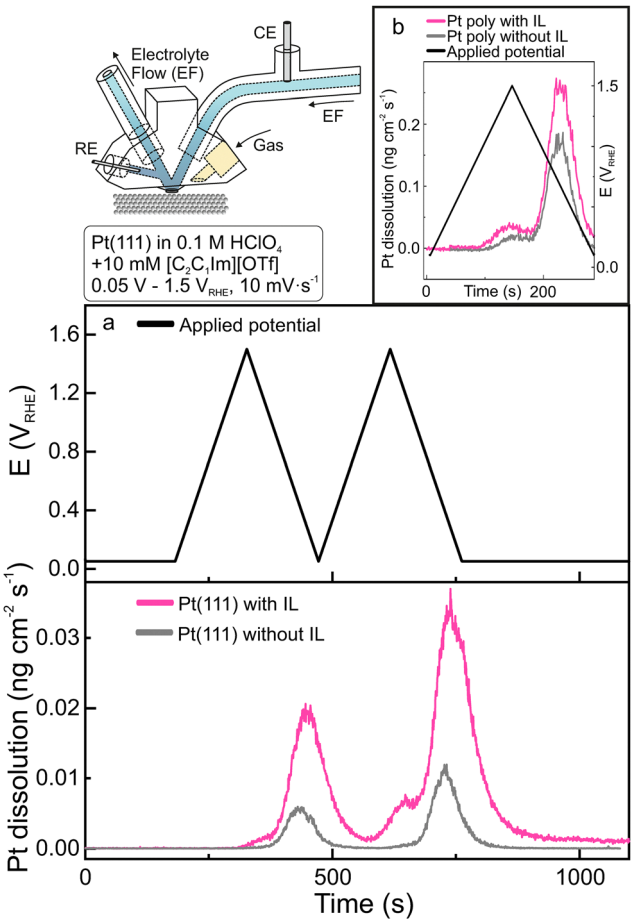

Fig. 3 (a) Online ICP-MS dissolution profiles for two consecutive CVs from Pt(111) in 0.1 M $HClO_4$ in the absence and presence of 10 mM [C_2C_1Im][OTf]. (b) Corresponding reference experiment of polycrystalline Pt. Applied electrochemical potential window 0.05–1.5 V_{RHE}, scan rate 10 mV s^{-1}.

ORCs (see discussion of the CVs), which has enhanced dissolution in the subsequent cycles. To explain the enhancement effect of the IL on the Pt dissolution, it is necessary to consider the influence of anions on the dissolution behavior in general. In previous work, some of the authors have shown that the nature of the present anion directly affects the dissolution. Specifically, the dissolution increases with increasing interaction strength of the anion following the order ClO_4^- < $CH_3SO_3^-$ < SO_4^{2-}.[39] However, the enhancement in dissolution observed in this work is significantly more pronounced suggesting that beside the stronger interaction of the IL with the Pt(111) surface,[23] an additional effect could play a role. Also, dissolved solutes will substantially influence the IL interface electrochemistry.[64,65] In previous work, we demonstrated that already low concentrations (10 mM) of the complexating IL [C_2C_1Im][DCA] increases the dissolution of Au(111) drastically (by a factor of more than 40).[22] Similar effects can also occur in the system investigated, here, even though the effect of the IL is much less pronounced in the current study. These results suggest that the dissolution behavior can be tuned by selecting different ionic liquids, partially due to their varying tendencies to form complexes.

EC-STM

While we observed a distinct influence of the IL on the dissolution behavior, its influence on the development of the facets formed during ORCs is only minor. The question remains, how the presence of the IL affects the final morphology formed during consecutive ORCs. To address this question, we conducted *in situ* EC-STM measurements between ORCs performed in the absence and the presence of the IL [C_2C_1Im][OTf]. We used the same experimental procedure as in the CV experiment. We cycled the potential in 0.1 M $HClO_4$ between 0.05 and 1.5 V_{RHE} at 50 mV s^{-1}. STM images were measured prior to cycling and after 1, 3, 10, 20 and 40 cycles to examine the initial progression of surface morphology. The resulting images are shown in Fig. 4, with corresponding enlargements in the square inlets.

Before the first ORC, we observe large, defect-lean (111) terraces for both environments. The height of individual terraces is ~0.24 nm, which is in agreement with literature for Pt(111).[66–68] Potential cycling leads to roughening of the Pt surface. After the first cycle, the surface roughness which was determined using the magnified insets shown in Fig. 4, has increased from 61 to 108 pm in absence of the IL and from 63 to 87 pm with IL present. Note that also in the characterization CVs, the peaks assigned to the formation of {110} and {100} steps were less pronounced when cycling in presence of the IL. After 3 cycles, the surface roughness has further increased for both systems. In presence of the IL, a homogenous nanostructure with islands of ~1 nm diameter has formed on the surface. This structure is not visible in the system in absence of the IL and is most likely an artifact of the lower resolution of this particular image. After 10 cycles the nanostructure is visible for both systems. The diameter of the islands has increased to ~2 nm and the RMS value increased to 218 pm in absence of the IL and 179 pm in presence of the IL. With further cycles, the size of the islands continues to increase, up to ~2.5 nm after 40 cycles for both systems. The size distribution of nanoislands for 10, 20 and 40 cycles is shown in Section 3 of the ESI.† Despite the roughening of the surface, the terrace structure remains visible. The observations are in agreement with previous STM studies on surface roughening of Pt(111) in acidic media.[66,68,69]

Jacobse *et al.* identified in previous work two different regimes of nanoisland formation: a 'nucleation and early growth' regime and a 'late growth' regime. The 'nucleation and early growth' takes place in the initial cycles. Small islands nucleate with monoatomic height, which grow in number. At the same time vacancy islands form, which are however, difficult to detect using STM. We assign the roughening observed at cycles <10 to this initial growth mode. At higher cycle numbers the nucleation and growth regime transforms into the late growth regime in which the nucleation stops and existing islands grow in 3 dimensions. Note that larger particles also expose {110} and {100} facet sites, which were also observed in the CV experiment. In the next step, we analyzed the development of morphology using a high number of ORCs. The experimental conditions were the same as for lower number of cycles, except for the sweep rate, which was set to 400 mV s^{-1}. Images were taken after 200, 400 and 800 cycles. After 200 cycles, the Pt surface is homogeneously

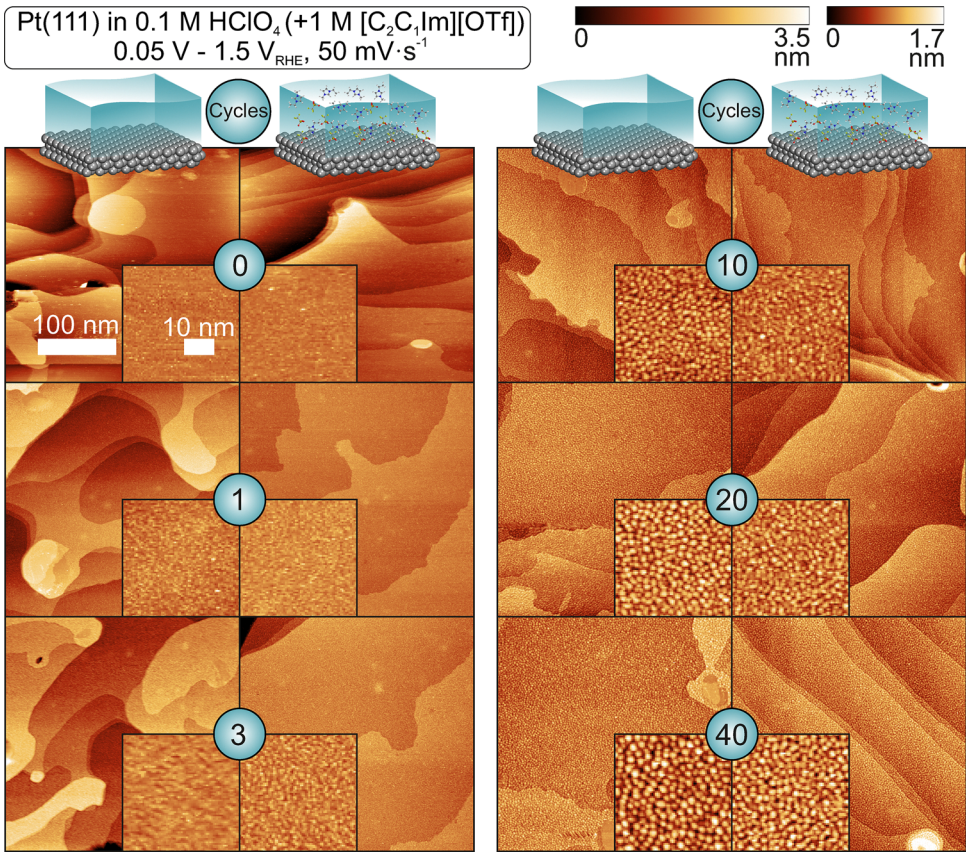

Fig. 4 EC-STM images (U_{bias} 0.4 V, I_t 0.2–1 nA) before and after the initial oxidation–reduction cycles (0.05–1.5 V_{RHE}, 50 mV s^{-1}) in the absence (left) and presence (right) of 1 M [C_2C_1Im][OTf]. Supporting electrolyte was 0.1 M $HClO_4$.

covered with nanoislands of similar size for both systems. With increasing cycle number, the particles grow. When comparing the system with and without IL, only minor differences are observed even after 800 cycles. This stands in clear contrast to our previous study on [C_2C_1Im][DCA] on Au(111), which revealed significant differences in the resulting morphology following ORC, depending on the presence of the IL.[22] These findings suggest that the influence of the IL is strongly dependent on the electrode material and/or the specific IL used. The pronounced effect of the IL is also consistent with the work by Endres *et al.*, who demonstrated that surface restructuring is highly sensitive to the nature of the IL.[30] To quantify the size of the formed islands in detail, we applied an algorithmic pattern recognition approach. The resulting distribution histograms are displayed in Fig. 6 and the obtained particle sizes are summarized in Table 1 (see ESI,† Section 3 for the corresponding data of the initial cycles). With increasing cycle number, the particle sizes increase and show a broader distribution. Finally, the peak shape and maxima between cycling in absence and presence of the IL are very close to each other. From CVs as well as the analysis of the STM images we conclude that the effect of the IL on the morphology is minimal, even though the IL affects significantly the Pt dissolution. In general, two effects shape the morphology during ORCs. On the one hand, the formation of the amorphous 3D oxide layer followed by its reduction leads to surface roughening because not all atoms reach the original position.[68,69] On the other hand, both Pt dissolution and the subsequent redeposition will change the surface structure. While the first process is mostly independent of the Pt dissolution, the second process depends strongly on it. The observation that the structural changes in the absence and the presence of the IL are literally the same, suggests that the morphological changes during ORC are strongly dominated by the first process, which is also in accordance with previous assumptions.[68,69]

Table 1 Mean particle sizes formed on Pt(111) after extended number of ORCs determined from STM images (shown in Fig. 5) using an algorithmic pattern recognition approach. The corresponding particle size distribution is shown in Fig. 6

Cycle number	Mean island size after ORC in the absence of IL (nm^2)	Mean island size after ORC in the presence of IL (nm^2)
200	6.3 ± 3.3	6.6 ± 3.1
400	8.5 ± 3.9	9.7 ± 4.8
800	12.8 ± 7.4	12.2 ± 6.8

Conclusions

We investigated the influence of the IL [C_2C_1Im][OTf] on the electrochemical stability of Pt(111) in 0.1 M $HClO_4$ in a potential window of 0.05–1.5 V_{RHE}. We compare experiments in

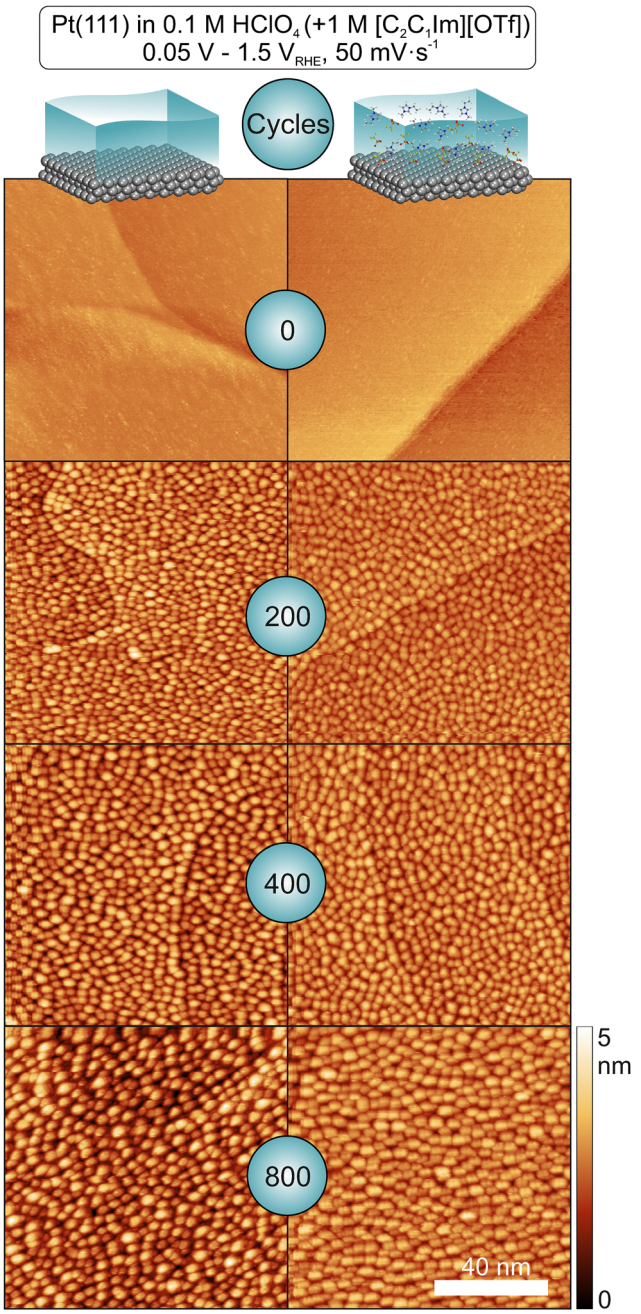

Fig. 5 EC-STM images (U_{bias} 0.4 V, I_t 0.2–1 nA) after extended ORCs (0.05–1.5 V_{RHE}, 400 mV s^{-1}) in the absence (left) and presence (right) of 1 M $[C_2C_1Im][OTf]$. Supporting electrolyte was 0.1 M $HClO_4$.

the presence of IL with reference experiments in the absence of IL. We used CV, online ICP-MS, and EC-STM in combination with an algorithmic pattern recognition approach to study the stability during ORCs. The results are summarized in the following:

(1) IL-surface interaction

$[OTf]^-$ ions of the IL $[C_2C_1Im][OTf]$ adsorb potential dependent on the Pt surface. This specific adsorption blocks partially the hydrogen and, in a more pronounced fashion, the OH adsorption.

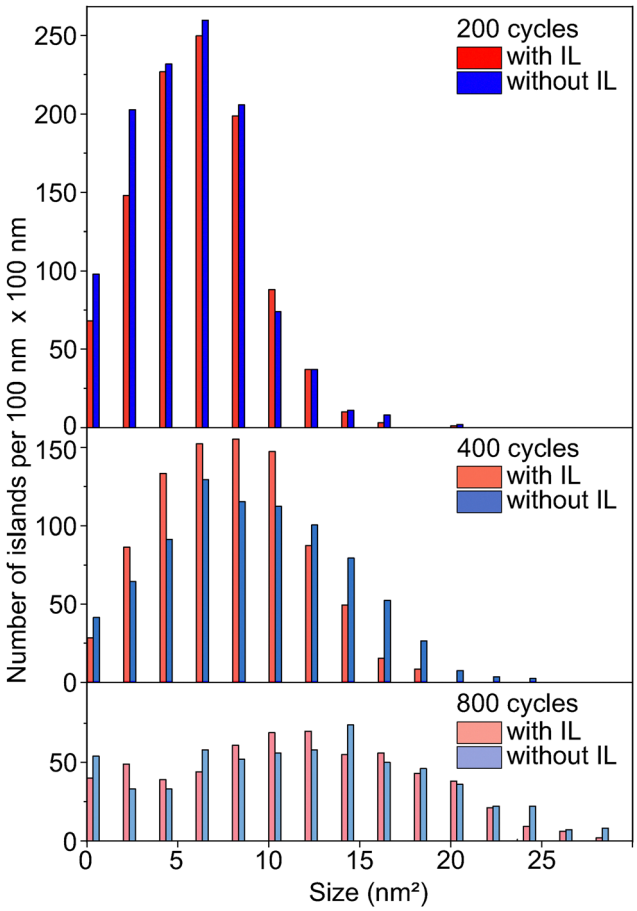

Fig. 6 Size distribution histogram of nanoislands in EC-STM images from Fig. 5. The corresponding values are summarized in Table 1.

This implies that the anions adsorb and block preferentially the low coordinated defect sites formed during the ORCs.

(2) Dissolution

In the absence of IL, Pt(111) dissolves almost exclusively during the cathodic process. In the consecutive cycle, the dissolution is increased, due to the formation of low coordinated adsorption sites, which dissolve more easily. In the presence of low concentrations of IL (10 mM), dissolution increases by factor of 5 and the onset of anodic dissolution appears at more negative potentials. We assign the increased dissolution to an anion effect and possibly also the formation of complexes, which prevent the dissolved species from redeposition.

(3) Morphology and adsorption sites

In the initial cycles (<10), we observe roughening, which we assign to nucleation and initial growth, and the number of nucleation sites increases. Specifically, {110} and {100} defects form in the first cycle. In the consecutive cycles, {110} defects form preferentially due to surface strain relaxation. At cycle numbers ≥ 10, the growth enters the late grow regime, in which the existing islands grow in three dimensions and the particle size distribution broadens. In this growth regime formation of

facet sites is observable. However, the IL does not affect substantially the development of the morphology and adsorption sites. For the potential window 0.05–1.5 V_{RHE}, the effect of surface restructuring is much greater than the effect of dissolution. We conclude that the morphological changes are dominated by the formation and subsequent reduction of an amorphous oxide layer, which is unaffected by the IL and not by dissolution and redeposition.

Our work shows the complexity of the influence of ionic liquids on stability. In order to understand how the modification of IL affects the stability at a molecular level, model studies with defined systems are essential.

Declaration of generative AI and AI-assisted technologies in the writing process

During the preparation of this work the authors used AI-assisted technologies in order to improve the language. After using this tool/service, the authors reviewed and edited the content as needed and take full responsibility for the content of the publication.

Author contributions

F. H.: conceptualization, formal analysis, investigation, visualization, writing – original draft; Y. Q.: formal analysis, investigation, visualization, writing – review & editing; L. L.: formal analysis, investigation, visualization, writing – review & editing; K. H.: formal analysis, investigation, writing – review & editing; N. T.: investigation, resources, writing – review & editing; P. W.: conceptualization, funding acquisition, project administration, resources, supervision, writing – review & editing; O. K.: conceptualization, formal analysis, funding acquisition, project administration, supervision, writing – review & editing; A. S. S.: conceptualization, formal analysis, funding acquisition, project administration, supervision, writing – review & editing; K. J. J. M.: funding acquisition, supervision, project administration, writing – review & editing; V. B. M.: conceptualization, formal analysis, supervision, writing – review & editing; S. C. conceptualization, formal analysis, supervision, writing – review & editing; O. B.: conceptualization, formal analysis, funding acquisition, project administration, supervision, writing – original draft; J. L.: conceptualization, formal analysis, funding acquisition, project administration, supervision, writing – review & editing.

Data availability

The data that support the findings of this study are presented in the manuscript and the ESI.† Source data are provided at Zenodo: https://doi.org/10.5281/zenodo.14748629.

Conflicts of interest

There are no conflicts of interest to declare.

Acknowledgements

The authors acknowledge financial support by the Deutsche Forschungsgemeinschaft (DFG) *via* Collaborative Research Centre SFB 1452-Catalysis at Liquid Interfaces (project 431791331) and by the DFG *via* projects 322419553, 431733372 and 453560721.

References

1 U. Kernchen, B. Etzold, W. Korth and A. Jess, Solid Catalyst with Ionic Liquid Layer (SCILL) – A New Concept to Improve Selectivity Illustrated by Hydrogenation of Cyclooctadiene, *Chem. Eng. Technol.*, 2007, **30**(8), 985–994, DOI: **10.1002/ceat.200700050**.

2 N. Szesni, R. Fischer, A. Hagemeyer, F. Großmann, J. Boyer, H. C. Hou, D. M. Lowe, C. Lugmair, M. Sun and M. Urbancic, (*Catalyst composition for selective hydrogenation with improved characteristics*, WO 2013/057244A1, 2013.

3 J. Snyder, T. Fujita, M. W. Chen and J. Erlebacher, Oxygen reduction in nanoporous metal–ionic liquid composite electrocatalysts, *Nat. Mater.*, 2010, **9**(11), 904–907, DOI: **10.1038/nmat2878**.

4 G. R. Zhang and B. J. M. Etzold, Emerging Applications of Solid Catalysts with Ionic Liquid Layer Concept in Electrocatalysis, *Adv. Funct. Mater.*, 2021, **31**(28), 2010977, DOI: **10.1002/adfm.202010977**.

5 S. Favero, I. E. L. Stephens and M. M. Titirici, Engineering the Electrochemical Interface of Oxygen Reduction Electrocatalysts with Ionic Liquids: A Review, *Adv. Energy Sustainability Res.*, 2020, **2**(1), 2000062, DOI: **10.1002/aesr.202000062**.

6 G.-R. Zhang, M. Munoz and B. J. M. Etzold, Boosting Performance of Low Temperature Fuel Cell Catalysts by Subtle Ionic Liquid Modification, *ACS Appl. Mater. Interfaces*, 2015, **7**(6), 3562–3570, DOI: **10.1021/am5074003**.

7 J. Snyder, K. Livi and J. Erlebacher, Oxygen Reduction Reaction Performance of [MTBD][beti]-Encapsulated Nanoporous NiPt Alloy Nanoparticles, *Adv. Funct. Mater.*, 2013, **23**(44), 5494–5501, DOI: **10.1002/adfm.201301144**.

8 M. Qiao, C. Tang, L. C. Tanase, C. M. Teodorescu, C. Chen, Q. Zhang and M.-M. Titirici, Oxygenophilic ionic liquids promote the oxygen reduction reaction in Pt-free carbon electrocatalysts, *Mater. Horiz.*, 2017, **4**(5), 895–899, DOI: **10.1039/C7MH00298J**.

9 M. George, G.-R. Zhang, N. Schmitt, K. Brunnengräber, D. J. S. Sandbeck, K. J. J. Mayrhofer, S. Cherevko and B. J. M. Etzold, Effect of Ionic Liquid Modification on the ORR Performance and Degradation Mechanism of Trimetallic PtNiMo/C Catalysts, *ACS Catal.*, 2019, **9**(9), 8682–8692, DOI: **10.1021/acscatal.9b01772**.

10 S. Ji, T. Li, Z.-D. Gao, Y.-Y. Song and J.-J. Xu, Boosting the oxygen evolution reaction performance of CoS_2 microspheres by subtle ionic liquid modification, *Chem. Commun.*, 2018, **54**(63), 8765–8768, DOI: **10.1039/C8CC05352A**.

11 T. N. Pham Truong, H. Randriamahazaka and J. Ghilane, Polymer Brushes Ionic Liquid as a Catalyst for Oxygen Reduction and Oxygen Evolution Reactions, *ACS Catal.*, 2018, **8**(2), 869–875, DOI: **10.1021/acscatal.7b03158**.

12 Q. Wang, Y. Gao, Z. Ma, Y. Zhang, W. Ni, H. A. Younus, C. Zhang, Z. Chen and S. Zhang, Supported ionic liquid phase-boosted highly active and durable electrocatalysts towards hydrogen evolution reaction in acidic electrolyte, *J. Energy Chem.*, 2021, **54**, 342–351, DOI: **10.1016/j.jechem.2020.06.012**.

13 G. Iijima, T. Kitagawa, A. Katayama, T. Inomata, H. Yamaguchi, K. Suzuki, K. Hirata, Y. Hijikata, M. Ito and H. Masuda, CO_2 Reduction Promoted by Imidazole Supported on a Phosphonium-Type Ionic-Liquid-Modified Au Electrode at a Low Overpotential, *ACS Catal.*, 2018, **8**(3), 1990–2000, DOI: **10.1021/acscatal.7b03274**.

14 P. Tamilarasan and S. Ramaprabhu, A polymerized ionic liquid functionalized cathode catalyst support for a proton exchange membrane CO_2 conversion cell, *RSC Adv.*, 2015, **5**(32), 24864–24871, DOI: **10.1039/C5RA03002A**.

15 T. Yang, J. Yang, X. Deng, E. Franz, L. Fromm, N. Taccardi, Z. Liu, A. Görling, P. Wasserscheid and O. Brummel, *et al.*, Modifying the Electrocatalytic Selectivity of Oxidation Reactions with Ionic Liquids, *Angew. Chem., Int. Ed.*, 2022, **61**(29), e202202957, DOI: **10.1002/anie.202202957**.

16 J. Yang, F. Haßfurther, F. Hilpert, Z. Hussain, T. Yang, N. Taccardi, P. Wasserscheid, O. Brummel and J. Libuda, C–C bond cleavage in the electrooxidation of 2,3-butanediol controlled by an ionic liquid modifier, *J. Catal.*, 2024, **435**, 115541, DOI: **10.1016/j.jcat.2024.115541**.

17 M. Kastenmeier, E. Franz, F. Waidhas, T. Yang, N. Taccardi, P. Wasserscheid, O. Brummel and J. Libuda, Competition of Acetone Reduction and Hydrogen Evolution on Pt Single Crystal Electrodes in the Absence and Presence of the Ionic Liquid $[C_2C_1Im][OTf]$, *J. Phys. Chem. C*, 2023, **127**(47), 22975–22983, DOI: **10.1021/acs.jpcc.3c06260**.

18 G.-R. Zhang, S.-D. Straub, L.-L. Shen, Y. Hermans, P. Schmatz, A. M. Reichert, J. P. Hofmann, I. Katsounaros and B. J. M. Etzold, Probing CO_2 Reduction Pathways for Copper Catalysis Using an Ionic Liquid as a Chemical Trapping Agent, *Angew. Chem., Int. Ed.*, 2020, **59**(41), 18095–18102, DOI: **10.1002/anie.202009498**.

19 T. Barth, W. Korth and A. Jess, Selectivity-Enhancing Effect of a SCILL Catalyst in Butadiene Hydrogenation, *Chem. Eng. Technol.*, 2017, **40**(2), 395–404, DOI: **10.1002/ceat.201600140**.

20 V. I. Pârvulescu and C. Hardacre, Catalysis in Ionic Liquids, *Chem. Rev.*, 2007, **107**(6), 2615–2665, DOI: **10.1021/cr050948h**.

21 H.-P. Steinrück and P. Wasserscheid, Ionic Liquids in Catalysis, *Catal. Lett.*, 2014, **145**(1), 380–397, DOI: **10.1007/s10562-014-1435-x**.

22 J. Yang, F. Hilpert, Y. Qiu, E. Franz, V. Briega-Martos, S. Cherevko, K. Mayrhofer, O. Brummel and J. Libuda, Interactions of the Ionic Liquid $[C_2C_1Im][DCA]$ with Au(111) Electrodes: Interplay between Ion Adsorption, Electrode Structure, and Stability, *J. Phys. Chem. C*, 2024, **128**(7), 2834–2843, DOI: **10.1021/acs.jpcc.3c07122**.

23 O. Brummel, F. Faisal, T. Bauer, K. Pohako-Esko, P. Wasserscheid and J. Libuda, Ionic Liquid-Modified Electrocatalysts: The Interaction of $[C_1C_2Im][OTf]$ with Pt(111) and its Influence on Methanol Oxidation Studied by Electrochemical IR Spectroscopy, *Electrochim. Acta*, 2016, **188**, 825–836, DOI: **10.1016/j.electacta.2015.12.006**.

24 M. Sobota, M. Happel, M. Amende, N. Paape, P. Wasserscheid, M. Laurin and J. Libuda, Ligand Effects in SCILL Model Systems: Site-Specific Interactions with Pt and Pd Nanoparticles, *Adv. Mater.*, 2011, **23**(22–23), 2617–2621, DOI: **10.1002/adma.201004064**.

25 J. Arras, E. Paki, C. Roth, J. Radnik, M. Lucas and P. Claus, How a Supported Metal Is Influenced by an Ionic Liquid: In-Depth Characterization of SCILL-Type Palladium Catalysts and Their Hydrogen Adsorption, *J. Phys. Chem. C*, 2010, **114**(23), 10520–10526, DOI: **10.1021/jp1016196**.

26 L. Winter, S. Trzeciak, C. C. Fernández, S. Massicot, T. Talwar, F. Maier, D. Zahn and H.-P. Steinrück, Tailoring the Selectivity of 1,3-Butadiene versus 1-Butene Adsorption on Pt(111) by Ultrathin Ionic Liquid Films, *ACS Catal.*, 2023, **13**(16), 10866–10877, DOI: **10.1021/acscatal.3c02126**.

27 G. R. Zhang, T. Wolker, D. J. S. Sandbeck, M. Munoz, K. J. J. Mayrhofer, S. Cherevko and B. J. M. Etzold, Tuning the Electrocatalytic Performance of Ionic Liquid Modified Pt Catalysts for the Oxygen Reduction Reaction via Cationic Chain Engineering, *ACS Catal.*, 2018, **8**(9), 8244–8254, DOI: **10.1021/acscatal.8b02018**.

28 Y. Li, J. Hart, L. Profitt, S. Intikhab, S. Chatterjee, M. Taheri and J. Snyder, Sequential Capacitive Deposition of Ionic Liquids for Conformal Thin Film Coatings on Oxygen Reduction Reaction Electrocatalysts, *ACS Catal.*, 2019, **9**(10), 9311–9316, DOI: **10.1021/acscatal.9b03157**.

29 K. Huang, T. Song, O. Morales-Collazo, H. Jia and J. F. Brennecke, Enhancing Pt/C Catalysts for the Oxygen Reduction Reaction with Protic Ionic Liquids: The Effect of Anion Structure, *J. Electrochem. Soc.*, 2017, **164**(13), F1448, DOI: **10.1149/2.1071713jes**.

30 R. Atkin, S. Z. El Abedin, R. Hayes, L. H. S. Gasparotto, N. Borisenko and F. Endres, AFM and STM Studies on the Surface Interaction of [BMP]TFSA and [EMIm]TFSA Ionic Liquids with Au(111), *J. Phys. Chem. C*, 2009, **113**(30), 13266–13272, DOI: **10.1021/jp9026755**.

31 N. Borisenko, S. Zein El Abedin and F. Endres, In Situ STM Investigation of Gold Reconstruction and of Silicon Electrodeposition on Au(111) in the Room Temperature Ionic Liquid 1-Butyl-1-methylpyrrolidinium Bis(trifluoromethylsulfonyl)imide, *J. Phys. Chem. B*, 2006, **110**(12), 6250–6256, DOI: **10.1021/jp057337d**.

32 F. Endres, S. Z. El Abedin and N. Borissenko, Probing Lithium and Alumina Impurities in Air- and Water Stable Ionic Liquids by Cyclic Voltammetry and In Situ Scanning Tunneling Microscopy, *Z. Phys. Chem.*, 2006, **220**(10), 1377–1394, DOI: **10.1524/zpch.2006.220.10.1377**.

33 C. Hohner, L. Fromm, C. Schuschke, N. Taccardi, T. Xu, P. Wasserscheid, A. Görling and J. Libuda, Adsorption Motifs and Molecular Orientation at the Ionic Liquid/Noble Metal Interface: $[C_2C_1Im][NTf_2]$ on Pt(111), *Langmuir*, 2021, **37**(43), 12596–12607, DOI: **10.1021/acs.langmuir.1c01900**.

34 H. Bühlmeyer, T. Talwar, R. Eschenbacher, J. Barreto, J. Hauner, L. Knörr, H.-P. Steinrück, F. Maier and J. Libuda, Surface

Chemistry of a [C_2C_1Im][OTf] (Sub)Wetting Layer on Pt(111): A Combined XPS, IRAS, and STM Study, *ACS Appl. Mater. Interfaces*, 2024, **16**(18), 24063–24074, DOI: **10.1021/acsami.4c02239**.

35 D. Blaumeiser, C. Schuschke, L. Fromm, N. Taccardi, S. Schötz, R. Eschenbacher, H. Bühlmeyer, T. Xu, T. Bauer and P. Wasserscheid, *et al.*, CO Permeability and Wetting Behavior of Ionic Liquids on Pt(111): An IRAS and PM-IRAS Study from Ultrahigh Vacuum to Ambient Pressure, *J. Phys. Chem. C*, 2021, **125**(28), 15301–15315, DOI: **10.1021/acs.jpcc.1c04043**.

36 R. Eschenbacher, J. Steffen, K. Farrugia, N. Taccardi, P. Wasserscheid, A. Görling and J. Libuda, Reactivity of a model SCILL: Influence of co-adsorbed [C_2C_1Im][OTf] on the dehydrogenation of dimethylamine on Pt(111), *Surf. Sci.*, 2024, **743**, 122453, DOI: **10.1016/j.susc.2024.122453**.

37 O. Kasian, S. Geiger, K. J. J. Mayrhofer and S. Cherevko, Electrochemical On-line ICP-MS in Electrocatalysis Research, *Chem. Rec.*, 2019, **19**(10), 2130–2142, DOI: **10.1002/tcr.201800162**.

38 V. Shkirskiy, F. D. Speck, N. Kulyk and S. Cherevko, On the Time Resolution of Electrochemical Scanning Flow Cell Coupled to Downstream Analysis, *J. Electrochem. Soc.*, 2019, **166**(16), H866–H870, DOI: **10.1149/2.1401915jes**.

39 V. Briega-Martos, T. Fuchs, J. Drnec, O. M. Magnussen and S. Cherevko, Effects of Anions and Surface Structure on Pt Single Crystal Dissolution in Acidic Electrolytes, *ChemElectroChem*, 2024, **11**(4), e202300554, DOI: **10.1002/celc.202300554**.

40 S. Cherevko, N. Kulyk and K. J. J. Mayrhofer, Durability of platinum-based fuel cell electrocatalysts: Dissolution of bulk and nanoscale platinum, *Nano Energy*, 2016, **29**, 275–298, DOI: **10.1016/j.nanoen.2016.03.005**.

41 M. Fleischmann and J. N. Hiddleston, A palladium-hydrogen probe electrode for use as a microreference electrode, *J. Phys. E: Sci. Instrum.*, 1968, **1**(6), 667, DOI: **10.1088/0022-3735/1/6/424**.

42 D. Friebel, C. Schlaup, P. Broekmann and K. Wandelt, Sulfidation of a Cu submonolayer at the Au(111)/electrolyte interface – An in situ STM study, *Surf. Sci.*, 2006, **600**(13), 2800–2809, DOI: **10.1016/j.susc.2006.05.007**.

43 C. Stumm, M. Bertram, M. Kastenmeier, F. D. Speck, Z. Sun, J. Rodríguez-Fernández, J. V. Lauritsen, K. J. J. Mayrhofer, S. Cherevko and O. Brummel, *et al.*, Structural Dynamics of Ultrathin Cobalt Oxide Nanoislands under Potential Control, *Adv. Funct. Mater.*, 2021, **31**(13), 2009923, DOI: **10.1002/adfm.202009923**.

44 D. Nečas and P. Klapetek, Gwyddion: an open-source software for SPM data analysis, *Open Phys.*, 2012, **10**(1), 181–188, DOI: **10.2478/s11534-011-0096-2**.

45 K. Domke, E. Herrero, A. Rodes and J. M. Feliu, Determination of the potentials of zero total charge of Pt(100) stepped surfaces in the [011] zone. Effect of the step density and anion adsorption, *J. Electroanal. Chem.*, 2003, **552**, 115–128, DOI: **10.1016/s0022-0728(02)01471-7**.

46 A. Berna, V. Climent and J. Feliu, New understanding of the nature of OH adsorption on Pt(111) electrodes, *Electrochem. Commun.*, 2007, **9**(12), 2789–2794, DOI: **10.1016/j.elecom.2007.09.018**.

47 A. M. Gómez-Marín and J. M. Feliu, Pt(111) surface disorder kinetics in perchloric acid solutions and the influence of specific anion adsorption, *Electrochim. Acta*, 2012, **82**, 558–569, DOI: **10.1016/j.electacta.2012.04.066**.

48 M. T. M. Koper and J. J. Lukkien, Modeling the butterfly: the voltammetry of $(\sqrt{3} \times \sqrt{3})R30^\circ$ and p(2 × 2) overlayers on (111) electrodes, *J. Electroanal. Chem.*, 2000, **485**(2), 161–165, DOI: **10.1016/S0022-0728(00)00109-1**.

49 A. M. Gómez-Marín, J. Clavilier and J. M. Feliu, Sequential Pt(111) oxide formation in perchloric acid: An electrochemical study of surface species inter-conversion, *J. Electroanal. Chem.*, 2013, **688**, 360–370, DOI: **10.1016/j.jelechem.2012.07.016**.

50 Y.-F. Huang, P. J. Kooyman and M. T. M. Koper, Intermediate stages of electrochemical oxidation of single-crystalline platinum revealed by in situ Raman spectroscopy, *Nat. Commun.*, 2016, **7**(1), 12440, DOI: **10.1038/ncomms12440**.

51 C. Korzeniewski, V. Climent and J. M. Feliu, *Electrochemistry at Platinum Single Crystal Electrodes*, vol. 24, 2011, pp. 75–170.

52 I. T. McCrum, X. Chen, K. A. Schwarz, M. J. Janik and M. T. M. Koper, Effect of Step Density and Orientation on the Apparent pH Dependence of Hydrogen and Hydroxide Adsorption on Stepped Platinum Surfaces, *J. Phys. Chem. C*, 2018, **122**(29), 16756–16764, DOI: **10.1021/acs.jpcc.8b03660**.

53 M. J. T. C. van der Niet, N. Garcia-Araez, J. Hernández, J. M. Feliu and M. T. M. Koper, Water dissociation on well-defined platinum surfaces: The electrochemical perspective, *Catal. Today*, 2013, **202**, 105–113, DOI: **10.1016/j.cattod.2012.04.059**.

54 X. Chen, I. T. McCrum, K. A. Schwarz, M. J. Janik and M. T. M. Koper, Co-adsorption of Cations as the Cause of the Apparent pH Dependence of Hydrogen Adsorption on a Stepped Platinum Single-Crystal Electrode, *Angew. Chem., Int. Ed.*, 2017, **56**(47), 15025–15029, DOI: **10.1002/anie.201709455**.

55 R. Rizo, J. Fernández-Vidal, L. J. Hardwick, G. A. Attard, F. J. Vidal-Iglesias, V. Climent, E. Herrero and J. M. Feliu, Investigating the presence of adsorbed species on Pt steps at low potentials, *Nat. Commun.*, 2022, **13**(1), 2550, DOI: **10.1038/s41467-022-30241-7**.

56 R. Rizo, L. Chico-Mesa, R. M. Arán-Ais, V. Climent, E. Herrero and J. M. Feliu, Analysis of the OH Coverage on Low-Coordinated Pt Sites at Low Potentials, *ACS Electrochem.*, 2024, **1**(3), 351–359, DOI: **10.1021/acselectrochem.4c00107**.

57 K. Doblhoff-Dier and M. T. M. Koper, Electric double layer of Pt(111): Known unknowns and unknown knowns, *Curr. Opin. Electrochem.*, 2023, **39**, 101258, DOI: **10.1016/j.coelec.2023.101258**.

58 V. Gámez, G. Melle, V. Climent, R. M. Arán-Ais, E. Herrero and J. M. Feliu, New understanding of the voltammetry of platinum in non-adsorbing electrolytes, *Electrochim. Acta*, 2025, **512**, 145494, DOI: **10.1016/j.electacta.2024.145494**.

59 O. Brummel, F. Waidhas, I. Khalakhan, M. Vorokhta, M. Dubau, G. Kovács, H. A. Aleksandrov, K. M. Neyman, V. Matolín and J. Libuda, Structural transformations and

adsorption properties of PtNi nanoalloy thin film electrocatalysts prepared by magnetron co-sputtering, *Electrochim. Acta*, 2017, **251**, 427–441, DOI: 10.1016/j.electacta.2017.08.062.

60 A. F. B. Barbosa, V. Del Colle, A. M. Gómez-Marín, C. A. Angelucci and G. Tremiliosi-Filho, Effect of the Random Defects Generated on the Surface of Pt(111) on the Electro-oxidation of Ethanol: An Electrochemical Study, *ChemPhysChem*, 2019, **20**(22), 3045–3055, DOI: 10.1002/cphc.201900544.

61 H. P. Steinrück, J. Libuda, P. Wasserscheid, T. Cremer, C. Kolbeck, M. Laurin, F. Maier, M. Sobota, P. S. Schulz and M. Stark, Surface Science and Model Catalysis with Ionic Liquid-Modified Materials, *Adv. Mater.*, 2011, **23**(22–23), 2571–2587, DOI: 10.1002/adma.201100211.

62 A. A. Topalov, I. Katsounaros, M. Auinger, S. Cherevko, J. C. Meier, S. O. Klemm and K. J. Mayrhofer, Dissolution of platinum: limits for the deployment of electrochemical energy conversion, *Angew. Chem., Int. Ed.*, 2012, **51**(50), 12613–12615, DOI: 10.1002/anie.201207256.

63 T. Fuchs, V. Briega-Martos, J. Drnec, N. Stubb, I. Martens, F. Calle-Vallejo, D. A. Harrington, S. Cherevko and O. M. Magnussen, Anodic and Cathodic Platinum Dissolution Processes Involve Different Oxide Species, *Angew. Chem., Int. Ed.*, 2023, **62**(34), e202304293, DOI: 10.1002/anie.202304293.

64 F. Endres, N. Borisenko, S. Z. El Abedin, R. Hayes and R. Atkin, The interface ionic liquid(s)/electrode(s): In situSTM and AFM measurements, *Faraday Discuss.*, 2012, **154**, 221–233, DOI: 10.1039/C1FD00050K.

65 N. Borisenko, A. Lahiri, G. Pulletikurthi, T. Cui, T. Carstens, J. Zahlbach, R. Atkin and F. Endres, The Au(111)/IL interfacial nanostructure in the presence of precursors and its influence on the electrodeposition process, *Faraday Discuss.*, 2018, **206**, 459–473, DOI: 10.1039/C7FD00165G.

66 K. Itaya, S. Sugawara, K. Sashikata and N. Furuya, In-situ scanning tunneling microscopy of platinum (111) surface with the observation of monatomic steps, *J. Vac. Sci. Technol., A*, 1990, **8**(1), 515–519, DOI: 10.1116/1.576378.

67 K. Sashikata, N. Furuya and K. Itaya, In situ electrochemical scanning tunneling microscopy of single-crystal surfaces of Pt(111), Rh(111), and Pd(111) in aqueous sulfuric acid solution, *J. Vac. Sci. Technol., B:Microelectron. Nanometer Struct.--Process., Meas., Phenom.*, 1991, **9**(2), 457–464, DOI: 10.1116/1.585589.

68 L. Jacobse, Y. F. Huang, M. T. M. Koper and M. J. Rost, Correlation of surface site formation to nanoisland growth in the electrochemical roughening of Pt(111), *Nat. Mater.*, 2018, **17**(3), 277–282, DOI: 10.1038/s41563-017-0015-z.

69 M. Ruge, J. Drnec, B. Rahn, F. Reikowski, D. A. Harrington, F. Carlà, R. Felici, J. Stettner and O. M. Magnussen, Structural Reorganization of Pt(111) Electrodes by Electrochemical Oxidation and Reduction, *J. Am. Chem. Soc.*, 2017, **139**(12), 4532–4539, DOI: 10.1021/jacs.7b01039.

